The Journal of Physical Chemistry A

 VOLUME 103, NUMBER 28, JULY 15, 1999

ARTICLES

Triplet Energy Transfer within Closely Spaced Positional Isomers of Ru/Os Polypyridine-Based Heterodiads

Anthony Harriman,* Francisco M. Romero, and Raymond Ziessel

Laboratoire de Chimie, d'Electronique et de Photonique Moléculaires, Ecole Européenne de Chimie, Polymères et Matériaux, Université Louis Pasteur, 1 rue Blaise Pascal, B.P. 296, F-67008 Strasbourg, France

Andrew C. Benniston

Department of Chemistry, University of Glasgow, Glasgow G12 8QQ, United Kingdom

Received: October 30, 1998

A series of ditopic ligands has been synthesized in which terminal 2,2′-bipyridyl (bpy) groups are connected via an ethynylene group through different sites on the pyridine ring. These terminals have been capped with $[Ru(bpy)_2]^{2+}$ and $[Os(bpy)_2]^{2+}$ metallo-fragments to form photoactive heterodiads. In each case, quantitative intramolecular triplet energy transfer takes place along the molecular axis from the Ru-based terminal to its Os-based counterpart. Energy transfer, which is believed to involve through-bond electron exchange, is extremely fast and only slightly dependent on the geometry of the bridging ditopic ligand. Evaluation of vibronic overlap integrals, using Dexter-type formulism, or factors for the Franck−Condon weighted density of states, using Meyer's approach, allows estimation of the matrix elements for electron exchange. The two methods give comparable results, and it appears that electronic coupling within the triplet manifold is both modest and insensitive to the site at which the bridge is connected to the metal complexes. There exists a shallow relationship between the rate of electron exchange and the energy gap between triplets localized on donor and bridge, suggesting that this latter species participates in the energy-transfer process as a virtual state. Triplet energy transfer can also be considered in terms of a simultaneous two-electron, two-site exchange involving both LUMOs and HOMOs of the bridging ligand, with electron transfer through the LUMO being promoted by selective charge injection into the ditopic ligand under illumination. In this case, the products of the atomic orbital coefficients that describe coupling into and out of the bridge at the triplet level control the rate of energy transfer.

Triplet−triplet energy transfer, which might be important as a protective measure in natural photosynthetic organisms,[1] provides a convenient route by which to transfer stored information at the molecular level.[2] Many such molecular systems have been studied in recent years,[3−10] especially those cases where the donor and acceptor are transition metal polypyridine complexes,[11−16] with particular emphasis being given to molecular diads having the reactive terminals connected via an organic framework. Very fast rates of intramolecular triplet energy transfer have been reported for diads having the donor and acceptor units maintained in close proximity[9a,17] and/or linked by a conjugated spacer moiety.[16,18] Under such conditions, the most likely reaction pathway[5] involves through-bond electron exchange (i.e., Dexter-type energy transfer) although the intimate details of the mechanism have been investigated only rarely.

10.1021/jp9842805 CCC: $18.00
Published on Web 06/25/1999

In earlier work we reported rapid intramolecular triplet energy transfer from a ruthenium(II) bis(2,2′:6′,2″-terpyridyl)-based chromophore to a complementary osmium(II) bis(2,2′:6′,2″-terpyridyl)-based acceptor through a connecting alkynylene bridge.[16] We now extend this work to include the corresponding 2,2′-bipyridyl-based mixed-metal complexes having a single ethynylene group as the bridging unit. The advantage of these latter ditopic ligands is that it is easy to vary the site at which the ethynylene spacer is connected to the coordinated 2,2′-bipyridine ligand.[19] This approach provides access to three molecular heterodiads that retain similar thermodynamic properties but which differ with respect to the average distance (and the minimum number of bonds) between the metal centers. Additionally, the *ortho*-bridged isomer suffers from steric crowding around the cations that distorts the idealized octahedral geometry. The relevant reference compounds, both mono- and binuclear, were studied previously[20] in order to better understand the photophysical properties of these alkyne-substituted metal complexes. It was established that, following excitation with visible light, an electron is promoted from a metal center to the ditopic ligand, where it resides in an extended π^* orbital. This situation holds for both Ru^{II} and Os^{II} complexes and is likely to continue for the mixed-metal hybrids studied here.

Within the context of designing advanced prototypes of molecular-scale photoelectronic devices[21] it is necessary to identify and understand the factors that control the rates of energy transfer in these diads. This is the main rationale for the present investigation, which seeks to clarify the effect of connectivity on the rate of through-bond electron exchange. To expose this structural parameter, it is important to compare molecular diads exhibiting similar spectroscopic and thermodynamic properties. Whereas the relevant spectroscopic properties are easily evaluated in terms of Dexter theory,[22] calculating the thermodynamic properties is not so straightforward. Recent work by Meyer and co-workers,[10] however, has introduced a procedure based on emission spectral curve fitting[23] that facilitates estimation of the Franck−Condon factor for electron exchange. This procedure has been tested in several cases[9,10] and found to give a good representation of experimental findings while Razi Naqvi and Steel[24] have shown that a clear relationship exists between this Franck−Condon factor and the overlap integral calculated according to Dexter. These parameters, when used with the experimental rates of intramolecular electron exchange, allow independent estimation of the extent of electronic communication along the molecular axis in our diads. Such information is crucial for the design of improved and extended molecular models. Somewhat surprisingly, we show here that the site of attachment of the bridge has little influence on the ability of the ditopic ligand to support through-bond electron exchange.

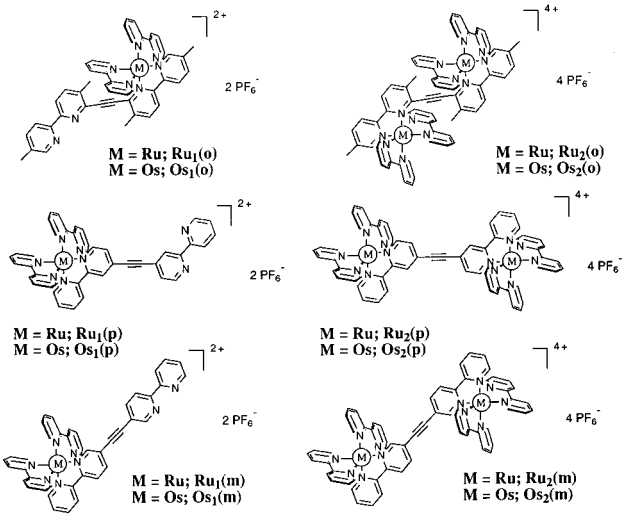

Figure 1. Structures of the mono- and homodinuclear reference compounds used in this work.

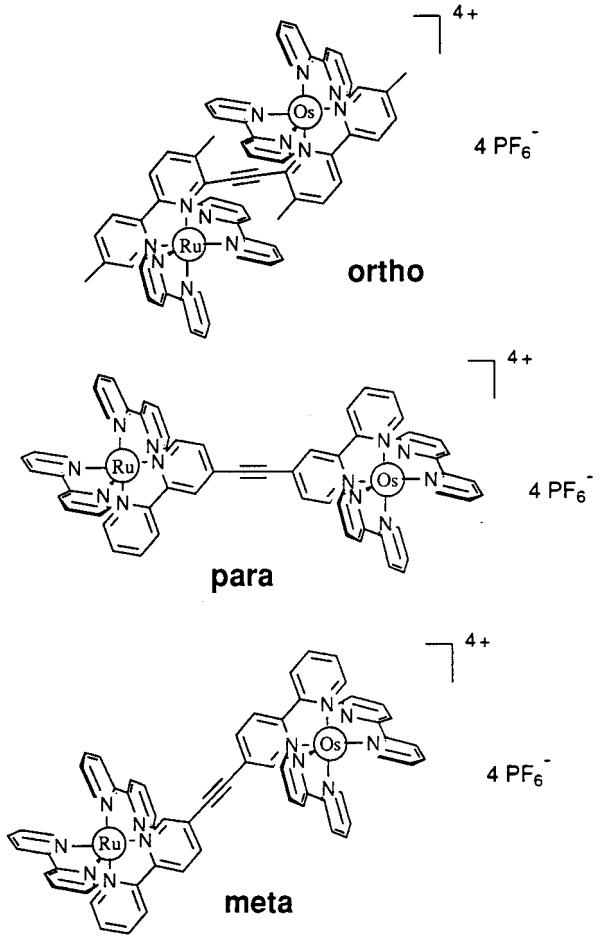

Figure 2. Structures of the various heterodiads.

Experimental Section

Materials. Reference compounds (Figure 1) were prepared and purified as described earlier,[20] while synthesis of the various ditopic ligands has been reported elsewhere.[19] The heterobinuclear Ru−Os complexes (Figure 2) were prepared by selective metalation of one end of the appropriate ditopic ligand[19] with 1 equiv of *cis*-$[Os(bpy)_2Cl_2]$[25] (bpy refers to 2,2′-bipyridine) followed by complexation of the vacant terminal with *cis*-$[Ru(bpy)_2Cl_2]\cdot 2H_2O$.[26] The alternative procedure of prior complexation with *cis*-$[Ru(bpy)_2Cl_2]\cdot 2H_2O$ gave significantly lower yields and risked introduction of trace amounts of luminescent impurities in the final sample. All complexes were purified as their chloride salts before isolation as the corresponding hexafluorophosphate salts. Analytical data are collected in Table 1 and fully support the assigned structures. In particular, electrospray mass spectrometry (ES-MS) provides a powerful methodology by which to characterize the new diads.[27] The spectra contain a series of pseudomolecular peaks corresponding to successive loss of PF_6^- anions, while the isotopic pattern measured at low accelerating voltage provides further confirmation of the assigned structure.

The mono-osmium(II) complexes were prepared by heating under reflux an Ar-purged solution of *cis*-$[Os(bpy)_2Cl_2]$ (0.089

TABLE 1: Selected Analytical Data for the Various Heterodiads

		ES-MS[a]		elemental composition	
diad	isolated yield (%)	found	calculated	calculated	found
ortho	65	1741.4	1741.4 $[M - PF_6]^+$	C 42.02	41.89
		798.1	798.2 $[M - 2PF_6]^{2+}$	H 2.89	2.67
		483.8	483.8 $[M - 3PF_6]^{3+}$	N 8.91	8.69
		326.6	326.6 $[M - 4PF6]^{4+}$		
meta	55	1685.3	1685.3 $[M - PF_6]^+$	C 40.69	40.47
		769.9	770.2 $[M - 2PF_6]^{2+}$	H 2.53	2.38
		464.7	465.1 $[M - 3PF_6]^{3+}$	N 9.18	9.01
		312.1	312.6 $[M - 4PF_6]^{4+}$		
para	56	1685.3	1685.3 $[M - PF_6]^+$	C 40.69	40.36
		770.0	770.2 $[M - 2PF_6]^{2+}$	H 2.53	2.28
		465.0	465.1 $[M - 3PF_6]^{3+}$	N 9.18	8.84
		312.5	312.6 $[M - 4PF_6]^{4+}$		

[a] Pseudomolecular peak obtained with an acceleration voltage of 20 V.

mmol) and the ditopic ligand (0.089 mmol) in ethanol (20 mL) until reaction was complete (2−4 days). After cooling to room temperature, the solvent was removed under vacuum and the residue was dissolved in CH_2Cl_2. The resultant solution was passed down a short column of alumina, using $CH_2Cl_2/CH_3OH = 9/1$ as eluant, to afford partial purification of the product. The required mono-osmium(II) complex was subsequently isolated by flash chromatography on silica using $CH_3CN/H_2O = 85/15$ as eluant and was recrystallized from CH_3CN/toluene by slow evaporation.

The purified mono-osmium(II) complex (0.067 mmol) was dissolved in Ar-purged ethanol (10 mL) and treated with *cis*-$[Ru(bpy)_2Cl_2]\cdot 2H_2O$ (0.067 mmol). The solution was heated to reflux overnight before removal of the solvent under vacuum. The residue was dissolved in CH_3CN and chromatographed on alumina, eluting with CH_3CN/H_2O 5/1 containing trace quantities of saturated aqueous NH_4Cl. The organic solvent was evaporated under vacuum and a solution of NH_4PF_6 (10 equiv) in water was added dropwise so as to precipitate the complex. The resultant solid was isolated, washed with water, and dried under vacuum. Analytically pure samples were obtained by slow diffusion of diethyl ether into an acetone solution of the complex.

Methods. Absorption spectra were recorded at ambient temperature with a Kontron Instruments Uvikon 930 spectrophotometer. Luminescence spectra were recorded in deoxygenated acetonitrile at 20 °C with a Perkin-Elmer LS50 spectrofluorometer equipped with a cooled R928 photomultiplier tube. The emission spectra were corrected for imperfections of the instrument by reference to a standard lamp. Only a small correction factor was required for wavelengths between 550 and 800 nm, but this factor became progressively more important between 800 and 900 nm. Emission maxima were reproducible to within ±5 nm. Quantum yields were calculated relative to ruthenium(II) and osmium(II) tris(2,2′-bipyridyl) complexes in acetonitrile,[28] using dilute solutions after deoxygenation by purging with argon. Luminescence quantum yields were taken as the average of three separate determinations and were reproducible to within ±8% but, because of the low emission probability for the osmium(II)-based chromophores, these derived quantum yields should be regarded as being approximate (i.e., ±25%).

Emission lifetimes were measured following excitation of the sample with a 30-ps laser pulse at 532 nm as delivered by a frequency-doubled, mode-locked Nd:YAG laser. The laser intensity was attenuated to 5 mJ per pulse, and incident pulses were defocused onto an adjustable pinhole positioned in front of the sample cuvette. Luminescence was collected with a microscope objective lens at 90° to excitation and isolated from any scattered laser light with nonemissive glass cutoff filters. The emergent luminescence was focused onto the entrance slit of a Spex high-radiance monochromator and thereby passed to a fast-response photomultiplier tube operated at 900 V. The output signal was transferred to a Tektronix SCD1000 transient recorder and subsequently to a microcomputer for storage and analysis. Approximately 500 individual laser shots, collected at 10 Hz, were averaged for kinetic measurements. The temporal resolution of this instrument, being determined by the rise time of the photomultiplier tube, was ca. 2 ns. Emission lifetimes measured with this setup were reproducible to within ±10%. All kinetic measurements were made with samples previously deoxygenated by purging with argon and the absorbance of each solution was adjusted to be ca. 0.08 at 532 nm. Data analysis was made by a nonlinear, least-squares iterative fitting routine that utilized a modified Levenberg−Marquardt global minimization procedure, after deconvolution of the instrument response function.[29]

Transient differential absorption spectra were recorded after excitation of the sample in deoxygenated acetonitrile with a 30-ps laser pulse at 532 nm. Where appropriate the excitation pulse was Raman shifted with perdeuterated cyclohexane to produce excitation wavelengths of 598 or 465 nm. The monitoring beam was provided by a pulsed, high-intensity Xe arc lamp passed through the sample at 90° to the excitation pulse. Spectra were compiled point-by-point, with five individual records being collected at each wavelength, using a Spex high-radiance monochromator operated with 2 nm slits. Kinetic measurements were made at fixed wavelength, with 300 individual laser shots being averaged for each decay profile. The time resolution of this setup was restricted to ca. 3 ns but was improved to ca. 50 ps by replacing the Xe monitoring beam with a pulse of white light generated by focusing residual laser light into a mixture of D_2O/H_2O. The excitation pulse was delayed with respect to that of the continuum with a computer-controlled optical delay stage and the two pulses were directed almost collinearly through the sample cell. The continuum pulse was split 50/50 before the sample cell so as to provide sample and reference beams. After passing through the sample, these beams were collected by fiber optics and analyzed with an image-intensified, Princeton dual-diode array spectrograph. The spectrometer was operated at 10 Hz, with 100 individual laser shots being averaged at each delay time. Baseline corrections were applied and emission was subtracted from the resultant spectra by recording control signals without the excitation or continuum pulses. Differential absorption spectra were corrected for distortions by reference to the optical Kerr effect obtained from CS_2.

Flash photolysis studies were also made with an Ar-ion pumped Ti-sapphire laser (Tsunami, Spectra Physics) operated at 820 nm (fwhm = 300 fs, 82 MHz, 450 mW). The output beam was split into two parts with approximately 80% and 20% of the total intensity, respectively. The frequency of the most intense beam was doubled with a 0.8 mm BBO crystal to produce pulses at 410 nm for use as the excitation source. The weaker beam was depolarized and focused into a 1 cm cuvette filled with water to produce a white light continuum for use as the analyzing pulse. The continuum was split into two equal beams before reaching the delay stage so as to provide a reference beam by which to normalize the transient absorption spectrum. This reference beam arrived at the sample cell ca. 1 ns before the excitation and analyzing beams; with the latter two pulses passing almost collinearly through the sample. Detection and data analysis were made as mentioned above.

Curve fitting of corrected emission spectra followed the procedure introduced by Meyer and co-workers.[10] Briefly, luminescence spectra recorded for the various reference compounds were corrected for spectral distortions of the instrument, reduced so as to display L/ν^3 vs ν where L is the luminescence intensity at wavenumber ν, and normalized.[23] Each spectrum was decomposed into three Gaussian-shaped bands of equal half-width, which gave a good representation of the complete spectrum, using the commercially available PEAKFIT program. The peaks were resolved using the second differential method with the Gaussian amplitude being set at 4%. From the individual Gaussian components it was possible to identify (i) the energy difference between 0,0 vibronic levels in the triplet and ground states (E_0), (ii) the average half-width at half-maximum ($\Delta\nu_{1/2}$) for the series of bands, and (iii) the average energy spacing between individual vibronic bands ($\hbar\omega$). These parameters were used to reconstruct the entire emission spectrum with MATHCAD V6, and the computed spectrum was compared to the experimental spectrum using the statistical analysis program SCIENTIST. The computed spectrum was then adjusted until the optimum match with the experimental spectrum was reached. Initially, the values of E_0 and $\Delta\nu_{1/2}$ were fixed, allowing refinement of $\hbar\omega$ and estimation of the electron-vibrational coupling constant S. Later, global refinement allowed E_0 to change but kept $\Delta\nu_{1/2}$ constant at the value obtained from the Gaussian analysis. To estimate the reorganization energy accompanying deactivation of the triplet state, $\Delta\nu_{1/2}$ was measured over a modest temperature range. Dexter overlap integrals were calculated[5,22] over the range $550 < \lambda < 900$ nm for reduced absorption and emission spectra.

PM3 RHF-SCF MO calculations for the S_0 and T_1 levels of the ditopic ligands were made with the MOPAC93 program package. For the configuration interaction calculations of the T_1 state, the two highest occupied (HOMO and HOMO-1) and two lowest unoccupied (LUMO and LUMO+1) orbitals were taken into consideration. Ab initio MO calculations for the triplet states were made on the protonated ditopic ligands at the CIS/3-21G level, while all other MO calculations were made for the free ligands after energy minimization of the structure using the AMBER force field. Estimates of the bond order of the nominally single and triple bonds in the bridge were made for energy-minimized structures of the π-radical anions of each ditopic ligand by comparing calculated bond lengths with the idealized structural parameters listed by Pauling.[30] Reduction potentials were taken from earlier work.[20]

Results and Discussion

Absorption and Emission Spectra. The three molecular heterodiads investigated here are expected to display intramolecular triplet energy transfer from the "Ru-bpy" fragment to the appended "Os-bpy" terminal. On the basis of earlier work,[16,18] we expect energy transfer to occur by way of through-bond electron exchange and the main purpose of this study is to evaluate how structural changes to the bridging unit affect the degree of electronic coupling along the molecular axis. First, it is necessary to demonstrate that intramolecular energy transfer does indeed take place in these systems, and this can be done most conveniently by examination of absorption and emission spectra recorded for the diads and for relevant reference compounds. For convenience, we refer to the ditopic ligands used to assemble these diads as being *ortho*, *meta*, or *para* according to the site at which the ethynylene bridge is attached with respect to the coordinated N atom (Figure 2). Similar behavior was noted for each isomer, and we outline the observed spectral characteristics by reference to the *meta* isomer, this being the most useful building block for construction of linear molecular arrays.[31]

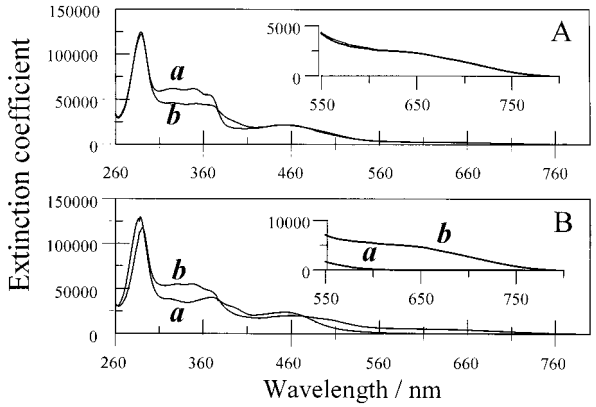

Figure 3. (A) Absorption spectra recorded for (a) the *meta*-heterodiad and (b) an equimolar mixture of $Ru_2(m)$ and $Os_2(m)$ with extinction coefficients being corrected appropriately. (B) Comparison of absorption spectra recorded for (a) $Ru_2(m)$ and (b) $Os_2(m)$ in acetonitrile. In each case, the inset shows an amplification of the far-red region of the spectrum.

The absorption spectrum recorded for the *meta* isomer in acetonitrile solution is shown in Figure 3A and shows several regions of interest. There is an intense π,π^* absorption band centered around 290 nm, which is due to ligand-centered transitions localized on the unsubstituted 2,2′-bipyridyl ligands. A series of weaker, but still intense, absorption bands can be resolved in the UV region between 300 and 380 nm that are associated with π,π^* transitions localized on the ditopic ligand. The region between 400 and 540 nm contains contributions from numerous metal-to-ligand, charge-transfer (MLCT) transitions associated with each metal center, but it is not possible to resolve individual bands. At longer wavelengths, the spectrum shows the expected spin-forbidden singlet-to-triplet MLCT transitions for each metal center.[32] Comparison of absorption spectra recorded for the corresponding binuclear reference compounds, $Ru_2(m)$ and $Os_2(m)$, shows that the "Os-bpy" fragment can be selectively excited at $\lambda > 560$ nm, but there is no wavelength at which the "Ru-bpy" fragment is the predominant chromophore (Figure 3B). An interesting feature of this latter comparison concerns the prominence of the π,π^* transitions localized on the ditopic ligand, and it appears that these bands are both red-shifted and less intense for $Ru_2(m)$ than for $Os_2(m)$. We interpret this effect to mean that electronic coupling is more significant in $Ru_2(m)$ since the excited-state manifold is known[20,33] to possess more charge-transfer character than that of $Os_2(m)$. The absorption spectrum of the *meta*-heterodiad closely matches that of an equimolar mixture of $Ru_2(m)$ and

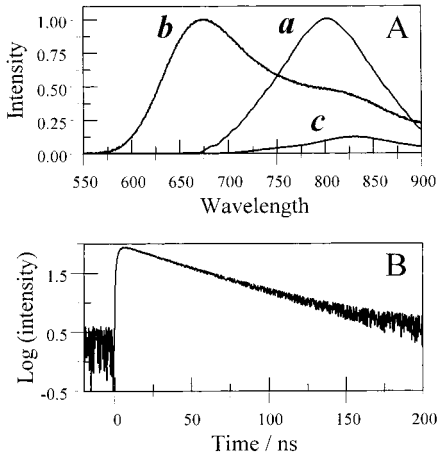

Figure 4. (A) Luminescence spectra recorded for (a) the *meta*-heterodiad and (b) an optically matched equimolar (ca. 5 μM) mixture of $Ru_1(m)$ and $Os_1(m)$ with excitation at an isosbestic point (470 nm). Small variations in the total concentration of the mixture indicate that bimolecular quenching is negligible under these conditions. Curve (c) shows the expected contribution made to the spectrum of the mixture by $Os_1(m)$. (B) Time-resolved emission decay profile recorded for the *meta*-heterodiad at 800 nm following laser excitation at 465 nm. The signal corresponds to a first-order process having a lifetime of 45 ± 3 ns.

$Os_2(m)$ across the entire spectral range, except where the spectrum is dominated by π,π^* transitions localized on the ditopic ligand (Figure 3A). These latter transitions are better resolved, more intense, and slightly blue shifted for the *meta*-heterodiad, suggesting that the terminals are less strongly coupled to the bridge than in $Ru_2(m)$. Consequently, it seems likely that the mononuclear complexes $Ru_1(m)$ and $Os_1(m)$ might serve as more appropriate reference compounds for photophysical investigations.

Illumination of the *meta*-heterodiad at any wavelength gives rise to emission from the "Os-bpy" fragment without obvious contamination by luminescence from the "Ru-bpy" chromophore (Figure 4). Luminescence from the "Os-bpy" unit, which is centered around 800 nm, clearly resembles that of the reference compound $Os_1(m)$ but any contribution from the "Ru-bpy" fragment cannot be resolved from the baseline. On the basis of the spectral properties of $Ru_1(m)$, we would expect to see emission from the "Ru-bpy" unit in the region around 650 nm but, relative to an optically matched, equimolar (ca. 5 μM) mixture of reference compounds where bimolecular interactions are negligible, this emission is quenched by >99%. Furthermore, the corrected excitation spectrum agrees well with the absorption spectrum recorded over the entire spectral range (Figure 5), especially the MLCT region, clearly indicating that photons absorbed by the "Ru-bpy" chromophore are channeled to the appended "Os-bpy" unit. These findings strongly support the idea of quantitative intramolecular energy transfer from the "Ru-bpy" fragment to the ethynylene-linked "Os-bpy" unit, followed by radiative and nonradiative decay of the triplet state localized on the latter unit.

The emission maximum (λ_{LUM}) and quantum yield (λ_{LUM}) remain similar to those measured for $Os_1(m)$ (Table 2) while, regardless of excitation wavelength, emission from the "Os-bpy" fragment was found to decay via monoexponential kinetics. The derived triplet lifetime (τ_T), as measured in deoxygenated acetonitrile, also remains closely comparable to that recorded for the reference compound (Table 2), such that there is no indication that the triplet state of the "Os-bpy" terminal is quenched in the heterodiads. The same behavior was found for

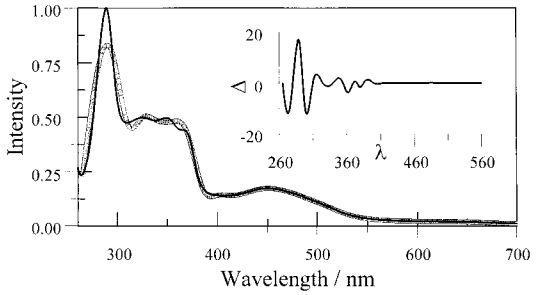

Figure 5. Comparison of absorption (solid line) and excitation (joined circles) spectra recorded for the *meta*-heterodiad. The emission wavelength was 800 nm. The inset shows the normalized difference (△), expressed as percentage, between the two spectra across the most important wavelength range. The apparent wavelength dependence seen for △ reflects the different slit widths used to record the two spectra.

TABLE 2: Photophysical Properties Recorded for the Reference Compounds and for the Various Heterodiads in Deoxygenated Acetonitrile at 20 °C

	"Ru-bpy"			"Os-bpy"		
complex	λ_{LUM}/nm[a]	Φ_{LUM}[b]	τ_T/ns[c]	λ_{LUM}/nm[a]	Φ_{LUM}[d]	τ_T/ns[c]
$Ru_1(o)$	612	0.0002	2.2			
$Ru_1(m)$	668	0.0470	1430			
$Ru_1(p)$	670	0.0390	1170			
$Os_1(o)$				755	0.0050	58
$Os_1(m)$				790	0.0041	40
$Os_1(p)$				785	0.0036	47
ortho	nd[e]		0.006	760	0.0042	38
meta	nd		0.004	800	0.0042	45
para	nd		0.017	800	0.0040	37

[a] Luminescence maximum, ±5 nm. [b] Luminescence quantum yield, ±10%. [c] Emission lifetime, ±5%. [d] ±25%. [e] nd = not detectable.

the *ortho* and *para* isomers, with the relevant photophysical properties being compiled in Table 2. Note that the ortho-substituted reference compound used to model the "Ru-bpy" fragment possesses an unusually short triplet lifetime. This is attributed to slight structural distortion around the metal center that increases interaction between the MLCT triplet and a higher-energy metal-centered state that is strongly coupled to the ground state. At 77 K, the triplet lifetime recorded for $Ru_1(o)$ is comparable to those measured for the other reference compounds.

Luminescence from the mononuclear reference compounds used to model the "Ru-bpy" fragment of the various heterodiads is easily detected and the photophysical properties are collected in Table 2. No such emission could be resolved for the heterodiads where, in particular, it was not possible to determine the triplet lifetime of the "Ru-bpy" fragment by time-resolved emission spectroscopy. These findings are fully consistent with quantitative triplet energy transfer along the molecular axis in each heterodiad occurring on the subnanosecond time range.

Laser Flash Photolysis Studies. Excitation of the *meta*-heterodiad with a 30-ps laser pulse at 598 nm, where the "Os-bpy" fragment absorbs ca. 97% of incident photons, gives a transient differential absorption spectrum characteristic of the triplet state of the "Os-bpy" terminal (Figure 6A). This species decayed via first-order kinetics with a lifetime (τ_T = 42 ± 5 ns) comparable to that measured by luminescence spectroscopy. Similar behavior was noted for the *ortho* and *para* isomers and confirms the above conclusion that the triplet state localized on the "Os-bpy" fragment remains relatively long-lived in the heterodiads. Laser excitation of these various heterodiads with a 30-ps laser pulse at 465 nm, where the "Ru-bpy" fragment absorbs ca. 50% of incident photons, also gave the differential

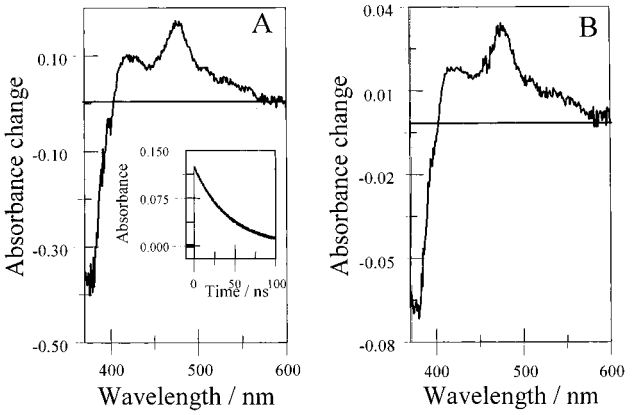

Figure 6. (A) Differential absorption spectrum recorded for the *meta*-heterodiad 100 ps after laser excitation at 598 nm. The inset shows a kinetics profile recorded at 480 nm that corresponds to a first-order decay with a lifetime of 42 ± 3 ns. (B) Transient differential absorption spectrum recorded 30 ps after laser excitation at 465 nm.

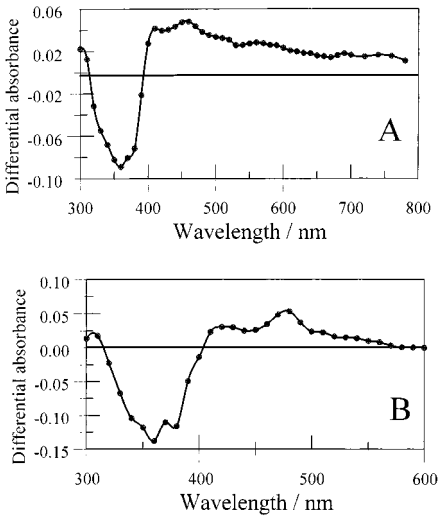

Figure 7. Transient differential absorption spectra recorded for (A) $Ru_1(m)$ and (B) $Os_1(m)$ after excitation with a 30-ps laser pulse at 532 nm. The spectra were recorded 10 ns after excitation.

absorption spectrum attributable to the "Os-bpy" fragment, even at the shortest delay times (Figure 6B). Indeed, the transient spectral records contained no indication for intermediate population of the triplet state localized on the "Ru-bpy" fragment, despite the fact that the two chromophores absorb equally at this wavelength. Although differential spectra recorded for the reference compounds (Figure 7) lack distinctive features, they are sufficiently different in the far red region for us to conclude that intramolecular triplet energy transfer must be complete within 50 ps.

Excitation of the heterodiads with a much shorter laser pulse (fwhm = 0.3 ps) at 410 nm, where the two chromophores possess comparable extinction coefficients, gave rise to a richer spectral pattern (Figure 8). The spectral records show that the triplet state localized on the "Os-bpy" fragment is the only transient species present at delay times longer than ca. 20 ps but an additional species is present on shorter time scales, which is most likely the triplet state of the "Ru-bipy" fragment. No other "intermediates" are apparent in the spectral records. Kinetic analysis is easiest at wavelengths longer than ca. 600 nm, where absorbance due to the triplet state of the "Ru-bpy" fragment provides the dominant signal. Here, appearance of the signal follows the temporal profile of the excitation pulse while the prepulse baseline is essentially restored within 20 ps or so

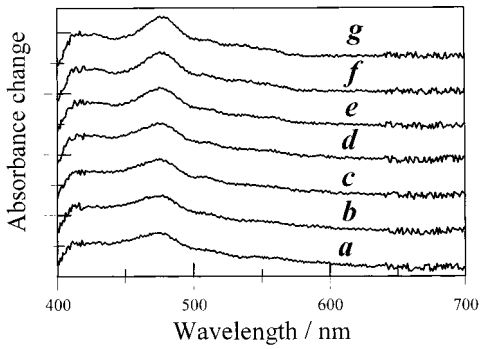

Figure 8. Transient differential absorption spectra recorded for the *meta*-heterodiad following excitation with a 0.3-ps laser pulse at 410 nm. Individual spectra were recorded at delay times of (a) 0.3, (b) 0.7, (c) 1.3, (d) 2, (e) 4, (f) 8, and (g) 20 ps. One division equals an absorbance change of 0.10.

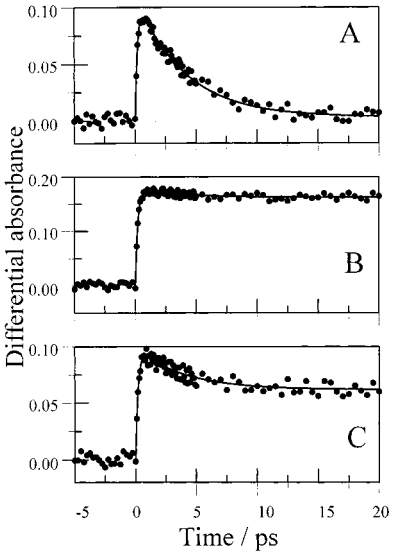

Figure 9. Decay profiles recorded at (A) 610 nm, (B) 480 nm, and (C) 430 nm following excitation of the *meta*-heterodiad with a 0.3-ps laser pulse at 410 nm. The solid line drawn through the data points corresponds to a first-order kinetic process with a lifetime of 4 ps.

(Figure 9A). The transient absorbance signal observed over the 600−700 nm region is well described in terms of the following expression

$$A(t) = A[\exp(-k_D t) - \exp(-k_F t)] \qquad (1)$$

where k_F and k_D, respectively, correspond to the first-order rate constants for formation and decay of the "Ru-bpy" triplet state. Deactivation of the triplet state is attributed to intramolecular triplet energy transfer from the "Ru-bpy" fragment to the corresponding "Os-bpy" unit and, since the triplet lifetime of the appropriate reference compound is ca. 1 μs, the rate constant for energy transfer ($k_{ET} = k_D$) can be derived by averaging kinetic traces collected over the 600−700 nm region (Table 3). Comparable behavior was found for the *ortho* and *para* isomers and the derived k_{ET} values remain similar (Table 3), although that found for the *para* isomer is distinctly smaller than the others.

Over the 400−600 nm range, the differential absorption spectral changes were consistent with initial formation of a mixture of triplet states associated with the two chromophores followed by rapid energy transfer to the "Os-bpy" fragment (Figure 8). Kinetic measurements made within this spectral window confirmed that the triplet state of the "Ru-bpy"

TABLE 3: Rate Constants and Calculated Spectroscopic Properties Related to Intramolecular Electron Exchange in the Various Heterodiads in Deoxygenated Acetonitrile at 20 °C

property	ortho	meta	para
$J_D/10^{-4}$ cm[a]	2.9	2.0	2.3
FC/10^{-4} cm[b]	2.3	1.9	1.6
λ_T/cm^{-1} [c]	3500	3200	3100
$-\Delta G°/cm^{-1}$ [d]	4400	2320	1950
$k_{ET}/10^{10}$ s^{-1} [e]	17	25	6
H_{DA}/cm^{-1} [f]	22	32	18
V_{DA}/cm^{-1} [g]	25	33	17

[a] Dexter overlap integral calculated from eq 2, ±10%. [b] Franck−Condon factor calculated according to eq 3, ±10%. [c] Total reorganization energy accompanying electron exchange, ±100 cm^{-1}. [d] Energy gap between first-excited triplet states localized on donor and acceptor, ±100 cm^{-1}. [e] Rate constant for intramolecular electron exchange, ±20%. [f] Matrix element for electron exchange calculated according to Dexter theory, ±20%. [g] Matrix element for electron exchange calculated according to nonadiabatic electron transfer theory, ±20%.

chromophore has a lifetime of (4 ± 1) ps for the *meta*-heterodiad while the signal due to the triplet state of the "Os-bpy" fragment did not decay on the picosecond time scale (Figure 9B,C). No wavelength could be found at which appearance of the "Os-bpy" triplet could be properly resolved and, in each case, the transient spectral records were dominated by fast decay of the triplet state localized on the "Ru-bpy" fragment. Averaging decay rates collected over the entire spectral range confirmed the k_{ET} values collected in Table 3. These values are extremely high, indicating the absence of any significant barriers to intramolecular electron exchange, and are similar to values reported earlier for related heterodiads.[9a,16,18] There is a 4-fold decrease in the rate of electron exchange for the *para* isomer relative to the *meta* analogue, while energy transfer in the *ortho* isomer is only slightly less efficient than that in the *meta* derivative.

Spectral Curve Fitting. The rate constant for through-bond electron exchange can be related to the Dexter overlap integral (J_D) between the normalized emission spectrum of the donor and the absorption spectrum of the acceptor.[5,22]

$$k_{ET} = \frac{2\pi}{\hbar} H_{DA}{}^2 J_D$$

$$J_D = \frac{\int L(\nu)\,\epsilon(\nu)\,d\nu}{\int L(\nu)\,d\nu \int \epsilon(\nu)\,d\nu} \qquad (2)$$

Here, L(ν) refers to the normalized reduced emission spectrum of the relevant mononuclear reference compound for the "Ru-bpy" fragment, expressed in terms of wavenumber (ν), and ϵ-(ν) is the reduced spectral distribution of the molar extinction coefficient of the corresponding reference compound for the "Os-bpy" fragment. The term H_{DA} is the matrix element for electron exchange between the triplet excited states of the terminal metal complexes. Evaluation of the overlap integral is straightforward, and the derived values are collected in Table 3. The values differ only slightly between the various isomers and follow the order *ortho* > *para* > *meta*. On the assumption that the measured rate constants refer exclusively to Dexter-type electron exchange, it now becomes possible to estimate the matrix elements (Table 3). Again, there is only slight variation among the isomers but the order is changed to *meta* > *ortho* > *para*. The size of these matrix elements is similar to that found for electron exchange in other mixed-metal diads and related complexes.[9a,10,16,17b]

The rate constant for electron exchange can also be expressed in terms of a nonadiabatic electron-transfer process using the formulism introduced by Marcus[34] and first applied to triplet energy transfer by Scandola and colleagues.[35] A more complete expression has been proposed by Meyer and co-workers[10] and subsequently tested by Schmehl et al.[9]

$$k_{ET} = \frac{2\pi}{\hbar} V_{DA}{}^2 FC$$

$$FC = \frac{1}{\sqrt{4\pi\lambda_T k_B T}} \sum_{n=0}^{\infty}\sum_{m=0}^{\infty} \exp(-S_D)\exp(-S_A)\left(\frac{S_D^n}{n!}\right)\left(\frac{S_A^m}{m!}\right)\exp(-\Delta G^*)$$

$$\Delta G^* = \left(\frac{(\Delta G° + \lambda_T + m\hbar\omega_D + n\hbar\omega_A)^2}{4\lambda_T k_B T}\right) \qquad (3)$$

Here, V_{DA} is the matrix element for electron exchange (nominally, $V_{DA} = H_{DA}$ but we prefer to separate these terms according to their origin), λ_T is the total reorganization energy accompanying electron exchange, k_B is the Boltzmann constant, and T is the absolute temperature. The terms S_A and S_D, respectively, refer to the electron-vibrational coupling constants for donor and acceptor while $\hbar\omega_D$ and $\hbar\omega_A$, respectively, are averaged medium-frequency vibronic modes coupled to the MLCT transition. The indices m and n are vibrational quantum numbers for donor and acceptor species, and in carrying out the summation, we have restricted these values to $m = n = 7$ since higher numbers had no effect on the calculated Franck−Condon factor (FC). The final term in the expression, $\Delta G°$, refers to the energy gap between the first-excited triplet states localized on donor and acceptor species. According to the treatment provided by Meyer and co-workers,[10] the various terms needed to calculate these Franck−Condon factors can be obtained from luminescence spectra recorded under appropriate conditions for donor and acceptor species.

Thus, the reduced emission spectrum,[23] as displayed in wavenumbers, of each reference compound was decomposed into three Gaussian-shaped components of equal half-width ($\Delta\nu_{1/2}$), since initial testing showed this to be sufficient to obtain a reliable and reproducible spectral analysis (Figure 10). The peak maximum (E_0) of the highest-energy Gaussian component is taken to represent the energy difference between 0,0 vibronic levels in the triplet and ground states while the averaged energy spacing between adjacent Gaussian components ($\hbar\omega$) is attributed to the averaged medium-frequency vibrational mode. The derived parameters are collected in Table 4 and were used to reconstruct the reduced luminescence spectrum according to

$$L(\nu) = \sum_{x=0}^{5}\left[\left(\frac{E_0 - x\hbar\omega}{E_0}\right)^3\left(\frac{S^x}{x!}\right)\left(\exp\left[-4\ln 2\left(\frac{\nu - E_0 + x\hbar\omega}{\Delta\nu_{1/2}}\right)^2\right]\right)\right] \qquad (4)$$

where the summation was restricted to $x = 5$. Iteration was continued until good agreement was reached between observed and calculated spectra, keeping $\Delta\nu_{1/2}$ at a constant value (Figure 10). This procedure allowed refinement of E_0 and $\hbar\omega$, although the final values remained within 5% of the initial estimates, and permitted estimation of the electron-vibrational coupling constants (S). The final computed values for these various parameters are collected in Table 4. The reorganization energy (λ) for each couple, assumed to contain contributions from both nuclear and solvent terms, was estimated from the temperature

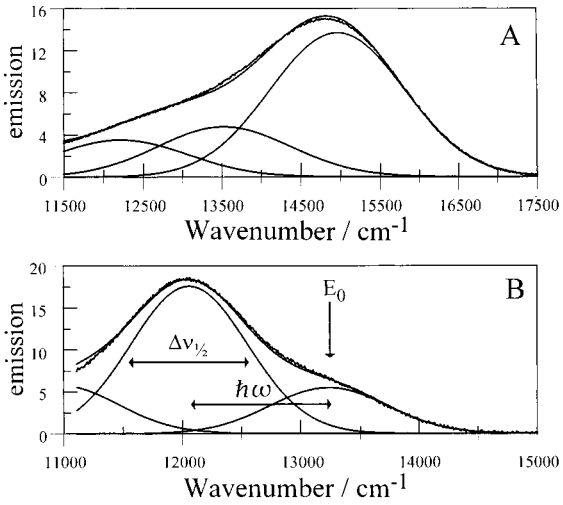

Figure 10. Illustration of the emission spectral curve fitting procedure used to derive the parameters listed in Table 4. Corrected emission spectra (noisy curves) are shown for (a) $Ru_1(m)$ and (b) $Os_1(m)$ with each full spectrum being decomposed into three Gaussian bands of constant half-width. The recalculated spectrum is shown as a solid line that overlays the experimental spectrum.

TABLE 4: Parameters Extracted from Fitting the Emission Spectra Recorded for the Mononuclear Reference Compounds in Deoxygenated Acetonitrile at 20 °C

cmpd	S^a	E_0/cm^{-1} ^{b}	λ/cm^{-1} ^{c}	$\hbar\omega$/cm^{-1} ^{d}	$\Delta\nu_{1/2}$/cm^{-1} ^{e}
Ru1(*o*)	0.92	16 500	2250	1460	2290
$Ru_1(m)$	0.56	15 000	1960	1460	2210
$Ru_1(p)$	0.56	15 050	1850	1490	2120
$Os_1(o)$	0.80	13 100	1250	1310	1690
$Os_1(m)$	0.55	13 400	1240	1350	1900
$Os_1(p)$	0.58	13 900	1150	1360	1620
$Ru_2(p)$	0.52	14 625	1800	1490	2030

[a] Electron-vibrational coupling constant, ±0.02. [b] Energy difference between (0,0) vibronic levels in the excited triplet and ground states, ±100 cm^{-1}. [c] Reorganization energy associated with formation of the lowest-energy excited triplet state, ±50 cm^{-1}. [d] Averaged medium-frequency vibrational mode coupled to the MLCT state, ±20 cm^{-1}. [e] Half-width of the Gaussian components derived by fitting the emission spectrum to a series of Gaussian-shaped bands, ±50 cm^{-1}.

dependence ($-20 < T < 50$ °C) of the averaged half-width of the Gaussian components according to

$$\lambda = \frac{(\Delta\nu_{1/2})^2}{16k_B T \ln(2)}$$

$$\lambda_T = \lambda_D + \lambda_A \qquad (5)$$

while the free energy change accompanying electron exchange was calculated as follows:

$$-\Delta G^\circ = (E_0^D + \lambda_D) - (E_0^A + \lambda_A) \qquad (6)$$

The derived parameters are collected in Table 3 and were used to calculate the Franck−Condon factors (FC) for electron exchange in the various heterodiads. In turn, these latter values were used to estimate the matrix elements for electron exchange (V_{DA}).

The spectroscopic parameters extracted from these fits indicate that intramolecular electron exchange is exoergic in each case and, since the total reorganization energy is comparable to the energy gap ($\lambda_T \approx -\Delta G^\circ$), reaction is likely to occur near the apex of a Marcus rate vs driving force profile.[34] Individual reorganization energies associated with triplet formation are quite small (Table 4), especially for the "Os-bpy" fragments where the triplet state possesses less charge-transfer character, while the averaged medium-frequency modes are in the range expected for C≡C, C═C, and C═N stretching modes. The electron-vibrational coupling constants vary considerably among the compounds but remain within the range normally found for luminescent transition metal polypyridine complexes.[9,10,20,25,28] The calculated Franck−Condon factors are in excellent agreement with the Dexter-type overlap integrals (Table 3).

Electronic Communication along the Molecular Axis. The fact that there exists good agreement between Dexter-type overlap integrals (J_D) and Franck−Condon weighted densities of state (FC) is a clear indication that intramolecular triplet energy transfer occurs predominantly via electron exchange. The derived matrix elements for electron exchange are modest and comparable to those estimated for other triplet energy-transfer processes, both bimolecular[10] and intramolecular.[9a,16,17b] This is surprising because the ethynylene bridge might be expected to provide an excellent conduit for electron and hole transfer between the terminal metal complexes.[16,18] A second unexpected aspect of this work is that the matrix element for electron exchange is not much affected by the structure of the ditopic ligand, despite the realization that the average metal−metal separation varies among the complexes and that stereochemical distortion is expected for the *ortho*-heterodiad. This relative insensitivity might arise from a fortuitous balancing of the factors that control V_{DA} (or H_{DA}) or from some kind of masking effect, as is often observed in bimolecular reactions.[36] Certainly, there are higher-energy triplet states localized on donor, acceptor, and bridge that could participate in the overall exchange mechanism. Of the two methods used to estimate the size of the matrix element, the Dexter approach is the more convenient and the most direct. It can be used in the present system because there is reasonably strong absorption by the Os-based acceptor over the relevant spectral range, but it is important to establish agreement with the Meyer approach since the latter can be used in cases where the acceptor is transparent.

Intramolecular electron exchange between donor (D) and acceptor (A) can be considered to involve virtual population of a triplet state localized on the bridge (S):

$$*(D)\sim\sim S\sim\sim A \rightarrow D\sim\sim(S)^*\sim\sim A \rightarrow D\sim\sim S\sim\sim(A)^*$$

As such, the magnitude of the matrix element for electron exchange will depend on the energy gap between triplet states localized on donor and bridge. The triplet energies of the bridging ligands are unknown but they are expected to be similar to that of 1,2-diphenylacetylene ($E_T = 21\,840$ cm^{-1})[37] and above that of the donor. To estimate these values, a set of molecular-orbital calculations was made at the CIS/3-21G level for the energy-minimized conformations of the protonated ditopic ligands.[38] These calculations indicate that the triplet energy of the bridging ditopic ligand decreases in the order *para* (E_T = 20 400 cm^{-1}) > *ortho* (E_T = 19 400 cm^{-1}) > *meta* (E_T = 17 500 cm^{-1}) so that the energy gap between donor and bridge triplets (ΔE_{TS}) follows the order *meta* ≈ *ortho* < *para* (Table 5). Since V_{DA} is expected to depend inversely on this energy gap, the above ordering gives a qualitative account of the experimental k_{ET} values. According to superexchange theory,[39]

$$V_{DA} = \frac{\alpha^2}{\Delta E_{TS}} \qquad (7)$$

where α represents the product of atomic orbital coefficients

TABLE 5: Parameters Associated with Electronic Coupling along the Molecular Axis in the Various Heterodiads or Ru-Based Reference Compounds

property	*ortho*	*meta*	*para*
$\Delta E_{TS}/cm^{-1}$ [a]	650	540	3400
α/cm^{-1} [b]	120	130	240
E_{LUMO}/eV [c]	−0.914	−1.092	−1.075
E_{RED}/V vs SCE [d]	−1.30	−1.22	−1.24
log K_D [e]	4.06	4.06	4.23
$N_{BO}(1)$ [f]	1.39	1.47	1.45
$N_{BO}(2)$ [g]	2.64	2.58	2.59
E_{HOMO}/eV [h]	−9.050	−8.911	−9.405
E_{OX}/V vs SCE [i]	1.42	1.40	1.38

[a] Energy gap between triplet states localized on the bridging ditopic ligand and the Ru(II)-based donor, ±10%. [b] Product of atomic orbital coefficients describing electronic coupling in to and out of the bridge at the triplet level, ±20%. [c] Calculated energy of the bridging LUMO, ±0.002 eV. [d] Reduction potential measured for addition of the first electron to the corresponding mononuclear Ru(II)-based reference compound, ±15 mV. [e] Disproportionation constant for the one-electron reduced binuclear Ru(II)-based reference compound, ±10%. [f] Bond order calculated for the [nominally] single bond in the bridging ethynylene group for the π-radical anion of the bridging ligand, ±0.01. [g] Bond order calculated for the [nominally] triple bond in the bridging ethynylene group for the π-radical anion of the bridging ligand, ±0.01. [h] Calculated energy of the bridging HOMO, ±0.002 eV. [i] Reduction potential measured for removal of an electron from the metal center of the corresponding mononuclear Ru(II)-based reference compound, ±15 mV.

describing coupling into and out of the bridge at the triplet level. Evaluation of this expression indicates that electronic coupling, as measured in terms of the α parameter (Table 5), increases in the order: *ortho* ≈ *meta* < *para*. It is also interesting to note that the calculated energy gaps are very small for the *ortho* and *meta* isomers, with the triplet state of the bridge being able to mix with that of the donor. Clearly, this situation is likely to promote rapid energy transfer along the molecular axis. Since the rate of energy transfer in the *para*-heterodiad is not much slower than that in the other isomers, we suppose that the much larger energy gap is offset by more effective orbital interaction.

Through-bond triplet energy transfer can also be considered in terms of a simultaneous two-electron, two-site exchange process involving electron transfer via the LUMO of the bridge and hole transfer through the bridging HOMO.[4] It has been demonstrated that the triplet excited states of the reference compounds[20] involve selective charge injection from metal center to the alkyne-substituted bpy, where the electron is delocalized over part of the ethynylene bridge. At the triplet level, therefore, the promoted electron is directed toward the molecular axis and this situation must be favorable for electron exchange. Furthermore, there is some suggestion that the extent of electronic coupling at the LUMO is comparable in the three isomers. Thus, the energy of the LUMO of the free ligand shows only a slight dependence on the site of attachment of the ethynylene bridge, as does the one-electron reduction potential measured for the mononuclear ruthenium(II) reference complexes (Table 5). The bond order for the first and central bonds in the ethynylene bridge, as calculated for the respective π-radical anions, is insensitive to the site at which the bridge is attached (Table 5) and indicates that each system adopts a partial cumulenic structure. There are also marked similarities in the size of the disproportionation constant (K_D) for the π-radical anions formed from the Ru(II) reference compounds,[20] as measured by cyclic voltammetry (Table 5). With respect to electron transfer through the bridging LUMO, therefore, these isomeric ditopic ligands are not expected to show disparate behavior.

In principle, the extent of electronic coupling between the metal centers can be estimated from analysis of intervalence charge-transfer (IVCT) absorption spectra measured for the mixed-valence complexes.[40] Such analysis depends critically on accurate knowledge of the distance separating the metal centers, but this term is hopelessly ambiguous in the complexes studied here. Consequently, although IVCT absorption bands can be seen in the near-infrared region, with peaks around 1400 nm, it has not been possible to extract meaningful coupling terms by fitting the bands to a Gaussian profile. Instead, we note that reduction potentials for oxidation of the metal center in the mononuclear Ru(II)-based reference compounds remain comparable for the three isomers while the HOMO of the *para* ditopic ligand lies at a lower energy that those of the other isomers. This means that the energy gap for hole transfer in the *para* isomer much exceeds those for the *ortho* and *meta* diads, thereby reflecting the trend in ΔE_{TS} values. On this basis, we surmise that it is the energetics of hole transfer that influence the extent of electronic coupling in these diads. It also follows that the enhanced electronic coupling implied for the *para* isomer operates for hole transfer not for electron transfer.

Concluding Remarks

This study has confirmed that an ethynylene bridge facilitates rapid through-bond electron exchange between photoactive terminals. The rates of intramolecular triplet energy transfer reported here are comparable to those found for related terpyridyl-based heterodiads[16,18] and for certain phenylene-bridged diads.[7d,17b] It is also shown that the matrix elements for electron exchange estimated by spectral analysis using methodologies introduced by Dexter[22] and by Meyer[10] are remarkably similar and that both sets of values appear realistic for triplet energy transfer. The Dexter method estimates spectral overlap between emission from the donor and absorption by the acceptor and provides the more reliable approach. The advantage of Meyer's method is that it uses only emission spectra and will be invaluable in those cases where the acceptor is transparent over the wavelength range of interest. It is further shown that, within this limited series of isomeric heterodiads, the geometry of the bridging ditopic ligand has little effect on the rate of energy transfer. This is a useful attribute with respect to constructing molecular arrays of different shapes since it suggests that longer molecules could be built by linking together different ditopic ligands without introducing a serious bottleneck into the system.

An interesting feature of this work is that the rate of through-bond electron exchange increases with decreasing energy gap between donor and bridge. This suggests that the rate of electron exchange could be optimized by structural modification of the bridge and an obvious way to do this is to extend the length of the central acetylenic function. Lowering the triplet energy in this way should partially offset the effect of increasing the separation distance between donor and acceptor moieties,[4] leading to an unusually small attenuation factor for electron exchange.[16] In fact, it is not necessary for the triplet energy of the bridge to exceed that of the donor. If the energy of the bridge triplet lies between those of the donor and acceptor, the bridge will appear as a real, as opposed to a virtual, intermediate. From this respect, it is plausible to consider ditopic ligands having up to four ethynylene groups as the central linkage.[2b]

An additional consequence of this work is that it permits some predictions to be made regarding triplet energy migration between the terminals of symmetrical "Ru-bpy" based homodiads. Thus, evaluation of eq 3 with the derived parameters listed

in Table 4 allows calculation of the FC factor for electron exchange between the terminals in $Ru_2(p)$ as being ca. 4.9×10^{-5} cm while, on the basis of eqn. 2, J_D has a value of ca. 3.6×10^{-5} cm for this system. Assuming a value for the matrix element for electron exchange of $V_{DA} = H_{DA} = 20$ cm^{-1}, the rate constant for triplet energy transfer in $Ru_2(p)$ is expected to be ca. 1.5×10^{10} s^{-1}. Since the triplet lifetime of $Ru_2(p)$ is 1.8 μs, it is reasonable to suppose that an equilibrium distribution of triplet states would be established in which, shortly after excitation, there is equal probability of finding the triplet on each terminal. Extending the molecular length by joining many "Ru-bpy" units into a linear array could lead to construction of compounds able to function as artificial light-harvesting arrays.

Acknowledgment. Financial support from ECPM, CNRS, and the Royal Society of London is gratefully acknowledged. We thank Johnson-Matthey PLC for their generous loan of precious-metal salts and Serge Wexler for recording the IVCT absorption spectra. We also thank Professor Hans Lami for the use of the variable temperature spectrofluorometer.

References and Notes

(1) (a) Monger, T. G.; Cogdell, R. J.; Parson, W. W. *Biochim. Biophys. Acta* **1976**, *449*, 136. (b) Davidson, E.; Cogdell, R. J. *Biochim. Biophys. Acta* **1981**, *635*, 295.

(2) (a) Balzani, V.; Scandola, F. *Supramolecular Photochemistry*; Horwood: Chichester, U.K., 1991. (b) El-ghayoury, A.; Harriman, A.; Hissler, M.; Ziessel, R. *Coord. Chem. Rev.* **1998**, *178−180*, 1251.

(3) (a) Gust, D.; Moore, T. A.; Moore, A. L.; Devadoss, C.; Liddell, P. A.; Hermant, R.; Nieman, R. A.; Demanche, L. J.; DeGraziano, J. M.; Gouni, I. *J. Am. Chem. Soc*. **1992**, *114*, 3590. (b) Sessler, J. L.; Wang, B.; Harriman, A. *J. Am. Chem. Soc*. **1995**, *117*, 704.

(4) (a) Closs, G. L.; Johnson, M. D.; Miller, J. R.; Piotrowiak, P. *J. Am. Chem. Soc*. **1989**, *111*, 3751. (b) Closs, G. L.; Piotrowiak, P.; MacInnis, J. M.; Fleming, G. R. *J. Am. Chem. Soc*. **1988**, *110*, 2652. (c) Sigman, M. E.; Closs, G. L. *J. Phys. Chem*. **1991**, *95*, 5012. (d) Closs, G. L.; Miller, J. R. *Science* **1988**, *240*, 440.

(5) (a) Levy, S. T.; Rubin, M. B.; Speiser, S. *J. Am. Chem. Soc*. **1992**, *114*, 10747. (b) Levy, S. T.; Speiser, S. *J. Chem. Phys*. **1992**, *96*, 3585.

(6) (a) Ford, W. E.; Rodgers, M. A. J. *J. Phys. Chem*. **1992**, *96*, 2917. (b) Wilson, G. J.; Sasse, W. H. F.; Mau, A. W.-H. *Chem. Phys. Lett*. **1996**, *250*, 583. (c) Wilson, G. J.; Launikonis, A.; Sasse, W. H. F.; Mau, A. W.-H. *J. Phys. Chem. A* **1997**, *101*, 4860. (d) Simon, J. A.; Curry, S. L.; Schmehl, R. H.; Schatz, T. R.; Piotrowiak, P.; Jin, X.; Thummel, R. P. *J. Am. Chem. Soc*. **1997**, *119*, 11012. (e) Thornton, N. B.; Schanze, K. S. *New. J. Chem*. **1996**, *20*, 791.

(7) (a) Indelli, M. T.; Bignozzi, C. A.; Harriman, A.; Schoonover, J. R.; Scandola, F. *J. Am. Chem. Soc*. **1994**, *116*, 3768. (b) Harriman, A.; Odobel, F.; Sauvage, J.-P. *J. Am. Chem. Soc*. **1994**, *116*, 5481. (c) Collin, J.-P.; Harriman, A.; Heitz, V.; Odobel, F. Sauvage, J.-P. *J. Am. Chem. Soc*. **1994**, *116*, 5679. (d) Indelli, M. T.; Scandola, F.; Collin, J.-P.; Sour, A.; Sauvage, J. P. *Inorg. Chem*. **1996**, *35*, 303.

(8) (a) Lee, E. J.; Wrighton, M. S. *J. Am. Chem. Soc*. **1991**, *113*, 8562. (b) Benniston, A. C.; Goulle, V.; Harriman, A.; Lehn, J.-M.; Marczinke, B. *J. Phys. Chem*. **1994**, *98*, 7798. (c) Wang, Y.; Schanze, K. S. *Inorg. Chem*. **1994**, *33*, 1354. (d) Larson, S. L.; Hendrickson, S. M.; Ferrere, S.; Derr, D. L.; Elliott, C. M. *J. Am. Chem. Soc*. **1995**, *118*, 2705. (e) MacQueen, D. B.; Eyler, J. R.; Schanze, K. S. *J. Am. Chem. Soc*. **1992**, *114*, 1897.

(9) (a) Liang, Y. Y.; Baba, A. I.; Kim, W. Y.; Atherton, S. J.; Schmehl, R. H. *J. Phys. Chem*. **1996**, *100*, 18408. (b) Shaw, J. R.; Sadler, G. S.; Wacholtz, W. F.; Ryu, C. K.; Schmehl, R. H. *New J. Chem*. **1996**, *20*, 749.

(10) (a) Murtaza, Z.; Zipp, A. P.; Worl, L. A.; Graff, D. K.; Jones, W. E., Jr.; Bates, W. D.; Meyer, T. J. *J. Am. Chem. Soc*. **1991**, *113*, 5113. (b) Murtaza, Z.; Graff, D. K.; Zipp, A. P.; Worl, L. A.; Jones, W. E., Jr.; Bates, W. D.; Meyer, T. J. *J. Phys. Chem*. **1994**, *98*, 10504.

(11) (a) Furue, M.; Yoshidzumi, T.; Kinoshiya, S.; Kushida, T.; Nozakura, S.; Kamachi, M. *Bull. Chem. Soc. Jpn*. **1991**, *64*, 1632. (b) Furue, M.; Kuroda, N.; Nozakura, S. *Chem. Lett*. **1986**, 1209.

(12) (a) Barigelletti, F.; Flamigni, L.; Balzani, V.; Collin, J.-P.; Sauvage, J.-P., Sour, A. *New J. Chem*. **1995**, *19*, 793. (b) De Cola, L.; Balzani, V.; Barigelletti, F.; Flamingi, L.; Belser, P.; von Zelewsky, A.; Franck, M.; Vögtle, F. *Inorg. Chem*. **1993**, *32*, 5298. (c) Barigelletti, F.; Flamigni, L.; Balzani, V.; Collin, J.-P.; Sauvage, J.-P.; Sour, A.; Constable, E. C.; Cargill-Thompson, A. M. W. *J. Am. Chem. Soc*. **1994**, *116*, 7692.

(13) (a) Strousse, G. F.; Worl, L. A.; Younathan, J. N.; Meyer, T. J. *J. Am. Chem. Soc*. **1989**, *111*, 9101. (b) Jones, W. E., Jr.; Baxter, S. M.; Mecklenburg, S. L.; Erickson, B. W.; Peek, B. M.; Meyer, T. J. In *Supramolecular Chemistry*; Balzani, V., De Cola, L., Eds.; Kluwer: Dordrecht, 1992; p 249.

(14) Guiffrida, G.; Calogero, G.; Ricevuto, V.; Campagna, S. *Inorg. Chem*. **1995**, *34*, 1957.

(15) (a) Grosshenny, V.; Harriman, A.; Hissler, M.; Ziessel, R. *J. Chem. Soc., Faraday Trans*. **1996**, *92*, 2223. (b) Grosshenny, V.; Harriman, A.; Hissler, M.; Ziessel, R. *Platinum Met. Rev*. **1996**, *40*, 26.

(16) Grosshenny, V.; Harriman, A.; Ziessel, R. *Angew. Chem., Int. Ed. Engl*. **1995**, *34*, 1100.

(17) (a) Kliner, D. A. V.; Tominga, K.; Walker, G. C.; Barbara, P. F. *J. Am. Chem. Soc*. **1992**, *114*, 8323. (b) Barigelletti, F.; Flamigni, L.; Balzani, V.; Collin, J.-P.; Sauvage, J.-P.; Sour, A.; Constable, E. C.; Cargill-Thompson, A. M. W. *J. Chem. Soc., Chem. Commun*. **1993**, 942.

(18) (a) Grosshenny, V.; Harriman, A.; Ziessel, R. *Angew. Chem., Int. Ed. Engl*. **1995**, *34*, 2705. (b) Benniston, A. C.; Harriman, A.; Grosshenny, V.; Ziessel, R. *New J. Chem*. **1997**, *21*, 405.

(19) Grosshenny, V.; Romero, F. M.; Ziessel, R. *J. Org. Chem*. **1997**, *62*, 1491.

(20) Grosshenny, V.; Harriman, A.; Romero, F. M.; Ziessel, R. *J. Phys. Chem*. **1996**, *100*, 17472.

(21) Harriman, A.; Ziessel, R. *Chem. Commun*. **1996**, 1707.

(22) Dexter, D. L. *J. Chem. Phys*. **1953**, *21*, 836.

(23) (a) Gould, I. R.; Noukakis, D.; Gomez-Jahn, L.; Young, R. H.; Goodman, J. L.; Farid, S. *Chem. Phys*. **1993**, *176*, 439. (b) Cortés, J.; Heitele, H.; Jortner, J. *J. Phys. Chem*. **1994**, *98*, 2527.

(24) Razi Naqvi, K.; Steel, C. *Spectrosc. Lett*. **1993**, *26*, 1761.

(25) Kober, E. M.; Caspar, J. V.; Sullivan, B. P.; Meyer, T. J. *Inorg. Chem*. **1988**, *27*, 4587.

(26) Sprintschnik, G.; Sprintschnik, H. W.; Kirsch, P. P.; Whitten, D. G. *J. Am. Chem. Soc*. **1977**, *99*, 4947.

(27) (a) Bitsch, F.; Hegy, G.; Dietrich-Buchecher, C. O.; Leize, E.; Sauvage, J.-P.; Van Dorsselaer, A. *New J. Chem*. **1994**, *18*, 801. (b) Hopfgartner, G.; Pigeut, C.; Henion, J. D. *J. Am. Soc. Mass Spectrom*. **1994**, *5*, 748. (c) Romero, F. M.; Ziessel, R.; Dupont-Gervais, A.; Van Dorsselaer, A. *Chem. Commun*. **1996**, 551.

(28) (a) Kober, E. M.; Marshall, J. L.; Dressick, W. J.; Sullivan, B. P.; Caspar, J. V.; Meyer, T. J. *Inorg. Chem*. **1985**, *24*, 2755. (b) Caspar, J. V.; Kober, E. M.; Sullivan, B. P.; Meyer, T. J. *J. Am. Chem. Soc*. **1982**, *104*, 630.

(29) Lami, H.; Piermont, T. *Chem. Phys*. **1992**, *163*, 149.

(30) Pauling, L. In *The Nature of the Chemical Bond*; Cornell: Ithaca, NY, 1990.

(31) Grosshenny, V.; Harriman, A.; Hissler, M.; Ziessel, R. *Platinum Met. Rev*. **1996**, *40*, 72.

(32) (a) Felix, F.; Ferguson, J.; Güdel, H. U.; Ludi, A. *J. Am. Chem. Soc*. **1980**, *102*, 4096. (b) Ferguson, J.; Krausz, E. *Inorg. Chem*. **1987**, *26*, 1383.

(33) Caspar, J. V.; Westmoreland, T. D.; Allen, G. H.; Bradley, P. G.; Meyer, T. J.; Woodruff, W. H. *J. Am. Chem. Soc*. **1984**, *106*, 3492.

(34) Marcus, R. A. *Discuss. Faraday Soc*. **1960**, *29*, 21.

(35) (a) Scandola, F.; Balzani, V. *J. Chem. Educ*. **1983**, *60*, 814. (b) Balzani, V.; Bolletta, F.; Scandola, F. *J. Am. Chem. Soc*. **1980**, *102*, 2152.

(36) (a) Scandola, F.; Balzani, V. *J. Am. Chem. Soc*. **1979**, *101*, 6140. (b) Razi Naqvi, K.; Steel, C. *Chem. Phys. Lett*. **1970**, *6*, 29. (c) Engel, P. S.; Fogel, L. D.; Steel, C. *J. Am. Chem. Soc*. **1974**, *96*, 327. (d) Wilkinson, F.; Familo, A. *J. Chem. Soc., Faraday Trans 2* **1976**, *72*, 604.

(37) Beer, M. *J. Chem. Phys*. **1956**, *25*, 745.

(38) Ngano, Y.; Ikoma, T.; Akiyama, K.; Tero-Kubota, S. *J. Phys. Chem*. **1998**, *102*, 5769.

(39) Larsson, S. *J. Am. Chem. Soc*. **1981**, *103*, 4034.

(40) (a) Hush, N. S. *Prog. Inorg. Chem*. **1967**, *8*, 391. (b) Creutz, C. *Ibid*. **1983**, *30*, 1.